Identification of postacute COVID-19 patterns in tomography using artificial intelligence

Identificação de padrões covid-19 pós-agudos em tomografia usando inteligência artificial

Identificación de patrones COVID-19 post-agudos en tomografía utilizando inteligencia artificial

Roberto Mogami[1], Carolina Gianella Cobo Chantong[2], Alexandra Maria Monteiro Grisolia[3], Breno Brandão Tavares[4], Otton Cavalcante Sierpe[4], Agnaldo José Lopes[1], Glenda Aparecida Peres dos Santos[5], Hanna da Silva Bessa da Costa[5], Karla Tereza Figueiredo Leite[6]

1 PhD/Professor, Radiology Department, State University of Rio de Janeiro, Rio de Janeiro (RJ), Brazil
2 MSc/M.D., Pedro Ernesto University Hospital, State University of Rio de Janeiro, Rio de Janeiro (RJ), Brazil
3 PhD/Professor, Program in Telemedicine and Telehealth, State University of Rio de Janeiro, Rio de Janeiro, Brazil.
4 Undergraduate Student, Mathematical and Statistics Institute, State University of Rio de Janeiro, Rio de Janeiro (RJ), Brazil
5 MSc Student/M.D., Radiology Department, State University of Rio de Janeiro, Rio de Janeiro, Brazil.
6 PhD/Associate Professor, Program in Telemedicine and Telehealth and Mathematical and Statistics Institute, State University of Rio de Janeiro, Rio de Janeiro, Brazil.

Autor correspondente: MSc Carolina Gianella Cobo Chantong
E-mail: gianella.cobo@gmail.com

Resumo

Objetivo: Desenvolver modelos de IA capazes de reconhecer padrões pulmonares pós-COVID em exames de tomografia computorizada. Método: Os radiologistas analisaram 87 exames de TC para estabelecer padrões tomográficos para treinar e testar modelos de aprendizagem profunda. O melhor modelo foi então selecionado para ler oito exames completos. Resultados: O modelo escolhido apresentou uma acurácia média de 92,21% na detecção de padrões pós-COVID.

Conclusão: Embora o tamanho da amostra fosse limitado, os testes com conjuntos de imagens e exames completos apresentaram resultados promissores. A amostra utilizada no estudo reflete o perfil epidemiológico encontrado na literatura.

Descritores: Síndrome de Pós-covid-19; Inteligência Artificial; Multidetectores para Tomografia Computorizada.

Abstract

Objective: Develop AI models capable of recognizing post-COVID lung patterns in computed tomography scans. Method: Radiologists analyzed 87 CT scans to establish tomographic patterns for training and testing deep learning models. The best model was then selected to read eight full scans. Results: The chosen model showed an average accuracy of 92.21% in detecting post-COVID patterns.

Conclusion: Although the sample size was limited, testing with image sets and full scans showed promising results. The sample used in the study reflects the epidemiological profile found in the literature.

Keywords: Postacute COVID-19 Syndrome; Artificial Intelligence; Multidetector Computed Tomography.

Resumen

Objetivo: Desarrollar modelos de IA capaces de reconocer patrones pulmonares post-COVID en tomografías computarizadas. Método: Los radiólogos analizaron 87 tomografías computarizadas para establecer patrones tomográficos para entrenar y probar modelos de aprendizaje profundo. Luego se seleccionó el mejor modelo para leer ocho escaneos completos. Resultados: El modelo elegido mostró una precisión promedio del 92,21% en la detección de patrones post-COVID.

Conclusión: Aunque el tamaño de la muestra fue limitado, las pruebas con conjuntos de imágenes y escaneos completos mostraron resultados prometedores. La muestra utilizada en el estudio refleja el perfil epidemiológico encontrado en la literatura.

Descriptores: Post aguda de COVID-19; Inteligencia artificial; Tomografía computarizada multidetector.

Introduction

The COVID-19 pandemic has been a significant event in recent world history, having catastrophic effects on public health. However, it has also led to the

development and improvement of new knowledge that has advanced several areas of science[1,2].

Three years after the pandemic began, there are concerns about the follow-up of infected patients, especially those who developed pulmonary complications due to prolonged hospitalization, mechanical ventilation use, and other health conditions. Postacute COVID-19 is a syndrome defined by the persistence of symptoms or complications related to COVID-19 more than four weeks after the onset of the disease that cannot be explained by other conditions[3,4]. These symptoms include dyspnoea, cough, and fatigue. In addition, radiological alterations can be observed on chest computed tomography (CT) as lesions similar to fibrosis [5, 6, 7].

The COVID-19 pandemic coincided with the fourth industrial revolution, when medicine benefited from combining machines with digital processes. This has revolutionized diagnostics and the prediction of complications and provided physicians with better solutions for problem-solving [8]. Artificial intelligence (AI) algorithms have played a crucial role in the acute phase of COVID-19 in diagnosing the disease, assessing pulmonary impairment, predicting severe forms, and identifying other causes of pulmonary disease [9, 10]. AI tools can detect pulmonary complications in the postacute phase and define various tomographic patterns associated with respiratory alterations [1, 9]. According to this premise, this group researched and developed AI models capable of identifying postacute COVID-19 chest tomographic patterns. In addition to the main objective, we also aimed to examine the radiological results of the exams used to create the models and to test these models on a group of post-COVID-19 patients. Also, It should be noted that no other studies related to the diagnosis of postacute COVID-19 by Machine Learning using images were found in the literature.

The rest of the paper is divided into three more sections. The Methods section presents related work and all the methodologies involved in the investigations to identify the best models for classifying postacute COVID-19 patterns. The Results section presents and discusses the performance of the models evaluated. Finally, the last section concludes and indicates the possibility of continuing the work.

Methods

Sample Selection

The authors selected 87 chest CT scans of patients diagnosed with postacute COVID-19 between July 2021 and May 2022 at the post-COVID outpatient clinic of the Policlínica Piquet Carneiro (PCC) of the State University of Rio de Janeiro (UERJ). To develop the models, the research group used 29 exams, and the best model among the investigated ones was tested with complete exams from eight patients. All patients in the study had their COVID-19 diagnosis confirmed through rRT-PCR tests. The researchers gathered information from electronic medical records and the RIS/PACS system of the Imaging Service at HUPE, UERJ. To be eligible for the study, patients needed to be over 18 years old, of any sex, and have had persistent respiratory symptoms for over four weeks after the onset of the disease. All exams were performed in inspiratory and expiratory apnoea. Patients were excluded from the study if their chest CT exams were of poor technical quality or if they had acute lung disease unrelated to COVID-19 that could explain their respiratory symptoms.

Computed Tomography

The medical team used inspiratory, expiratory, and high-resolution reconstruction (HRCT) techniques to conduct the chest CT scans. They utilized 64-channel multidetector equipment (Brilliance 40, Philips Medical Systems, Cleveland, OH, USA) with specific settings, including a reading time of four seconds, current of 458 mA, voltage of 120 kV, and thickness of two mm, with a distance between the slices of one mm. No iodinated contrast medium was used during the scans.

A group of four radiologists with more than ten years of chest radiology experience analysed the CT scans without any knowledge of the patient's clinical information. They looked for various abnormalities, including ground-glass opacities, crazy paving, consolidations, parenchymal bands, inverted halo pattern, halo sign, fibrosis-like lesions, peripheral vascular ectasia, and the presence of air trapping. After careful analysis, they classified the exams into preestablished tomographic patterns, including normal (NP), reabsorption (RP), small airway disease (SADP),

fibrosis-like lesions (FLLP), and nonspecific interstitial pneumonia-like lesions (NSIPP) [9].

Methodology for Building Models based on Artificial Intelligence

This study was based on two classical deep learning neural network architectures: VGG-11 [11] and MobileNetV2 [12]. The latter is a network developed by Google, which is very similar to the original MobileNet but has fewer parameters. Our decision to use these methodologies was based on preliminary experiments and the results found in related works [9]. These architectures had previously trained models, which allowed for transfer learning, a crucial factor given the limited number of images per pattern. Starting from scratch with such a small dataset would not have produced an adequate result [13, 14].

Database

We used a database of 2187 images from various patients to build the models. The distribution of slices between post-COVID-19 and normal patterns was as follows: PLSF: 355; PDPVA: 244; PLSPINE: 491; PR: 481; Normal pattern during inspiratory apnoea: 544 and Normal pattern during expiratory apnoea: 271.

Since the groups were unbalanced, we selected 40 images (approximately 10%) for validation and 40 images for testing (approximately 10%) from each group, leaving the rest for training. These images were kept separate for each step. The final model test was conducted using a set of slices not used in the development process.

The augmentation process was utilized to compensate for the limited number of training images, creating new images from the original ones. The conventional techniques of cropping, rotating, and translating were applied. However, the test dataset was not processed with this method [15, 16].

The Institutional Review Board of Hospital Universitario Pedro Ernesto (HUPE) approved the research with reference number 1363230.1.0000.5282. The consent form was waived, as only the hospital's database was used.

Models

It was developed three models using selected images (slices) of post-COVID-19 patterns. The objective was to evaluate the accuracy of these models in recognizing patterns in the slices. Next, the models were tested for pattern recognition in complete scans of eight patients. This second stage simulated a real-life situation where the model would be used to diagnose the type of pattern present in the tomography.

Two-Stage Model

The first model classified images in two stages using a hierarchical system. First, a neural network model was trained to differentiate between normal slices and those with post-COVID-19 characteristics, such as resorptive patterns, fibrosis-like lesions, NSIP-like lesions, and small airway disease. Slices classified as normal in the first stage were not analysed further in the second stage, which focused on identifying four post-COVID-19 patterns in the remaining slices.

Inspiration/Expiration Model

This model discriminated the post-COVID patterns using two submodels. One submodel analysed images taken with expiratory apnoea to evaluate small airway disease (SADP). The other submodel evaluated RP, FLLP, and NSIPP using images taken conventionally with inspiratory apnoea. The two submodels produced separate classifications but together identified all expected patterns on CT. The first submodel identified exams with and without small airway disease, while the second submodel differentiated normal exams from those with RP, SADP, FLLP, and NSIPP.

Single-Stage Model

The third model examined the slices and identified four post-COVID-19 patterns: RP, SADP, FLLP, and NSIPP. It was designed to classify only images with abnormal patterns to prioritize the model's efforts in distinguishing post-COVID-19 patterns.

Results

Sample Characterization

Out of the 29 patients whose images were used for this study, 19 were women (65.5%). The average age of the patients was 60, with a standard deviation of 13 years and a range of 35 to 88 years. On average, patients underwent radiological examinations 8.8 months after the onset of symptoms.

The most reported symptoms of postacute COVID-19 were dyspnoea and fatigue (82.4%) and cough (42.3%). Comorbidities were present in 23 patients (79.3%), with hypertension (58.6%) and diabetes mellitus (44.8%) being the most reported.

The most common CT findings were ground-glass opacities in 86.2% of patients, septal thickening in 62.1%, air trapping in 51.7%, parenchymal bands in 55.2%, bronchiectasis in 41.4%, peripheral vascular ectasia in 34.5%, subpleural lines in 34.5%, volumetric reduction in 13.8%, signs of bronchiolitis in 10.3%, crazy paving in 10.3%.

The CT scans revealed the following patterns: resorptive pattern (69%) (Fig. 1a), small airway disease pattern (31%) (Fig. 1b), fibrosis-like lesion pattern (24%) (Fig. 1c), a pattern of lesions similar to NSIP (10%) (Fig. 1d), and normal results (7%). Notably, some exams showed more than one pattern.

Figure 1 - Axial CT scan of the chest in the parenchyma window: Resorption pattern (a), showing ground-glass opacities in the subpleural regions(arrows); Small airway disease pattern (b), showing areas of air trapping (arrows); Fibrosis-like lesion pattern (c), showing reticular opacities associated with bronchial ectasias (arrows); Pattern of lesions similar to NSIPP (c), showing small subpleural reticular and ground-glass opacities

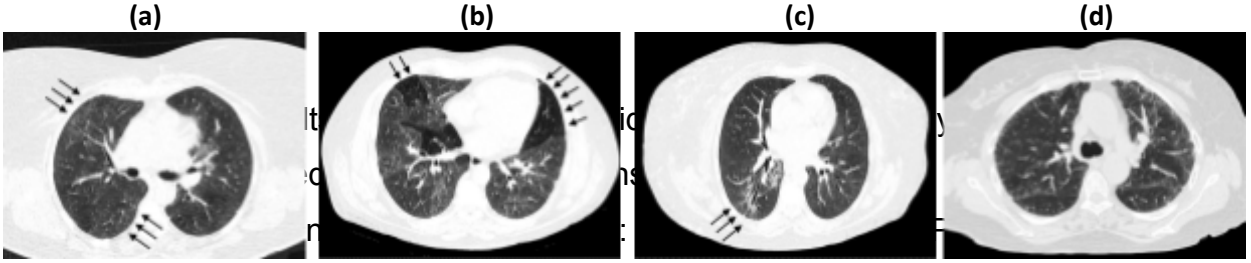

and RP; Patient seven: SADP and Patient eight: RP.

Two-Stage Model

During the initial stage of separating normal and post-COVID exams, the MobileNetV2 architecture was utilized, as it provided the best results. The accuracy values for training and validation were 97.47% and 96.59%, respectively, as shown in Fig. 2a. In Fig. 2b, the confusion matrix for the test phase is shown, which displays an accuracy of 96.59%, with only three errors out of 88 samples.

Figure 2 - Accuracy in the MobileNetV2 training and validation sets in the first layer of the hierarchical classification (97.47% in the 7th epoch) (a) and Confusion matrix of the MobileNetV2 test step in the first layer of the hierarchical classification (96.59%)(b)

(a) (b)

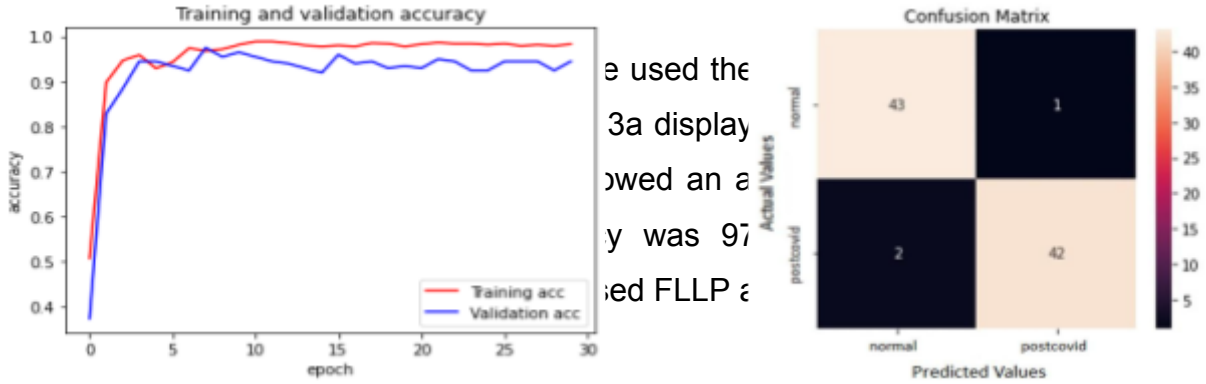

e used the
3a displa
owed an a
y was 97
ed FLLP a

Inspiration/Expiration Model

We utilized the MobileNetV2 design to analyse images in expiratory and inspiratory apnoea. Based on the graph illustrated in Fig. 4a, we achieved 99.7% and 99.0% accuracy in the training and validation stages, respectively, when categorizing images in expiratory apnoea. Fig. 4b displays the confusion matrix from the test phase, which had an accuracy of 90.8%. We observed that the model performed slightly worse (statistically) than the single-stage model during the test phase.

Regarding images in inspiratory apnoea, the training and validation graphs in Fig. 5a demonstrated accuracies of 99.91% and 98.0%, respectively. The test phase confusion matrix in Fig. 5b shows an accuracy of 99.6%.

Figure 3 – Accuracy and loss in the VGG-11 training and validation sets in the second layer of the hierarchical classification (97.96% in the 7th epoch) (a); Confusion matrix of the VGG-11 test step in the second layer of the hierarchical classification (97.73%). FLLP = fibrosis-like lesion pattern; NSIPP = nonspecific interstitial pneumonia pattern; RP = resorption pattern; SADP=small airway disease pattern (b)

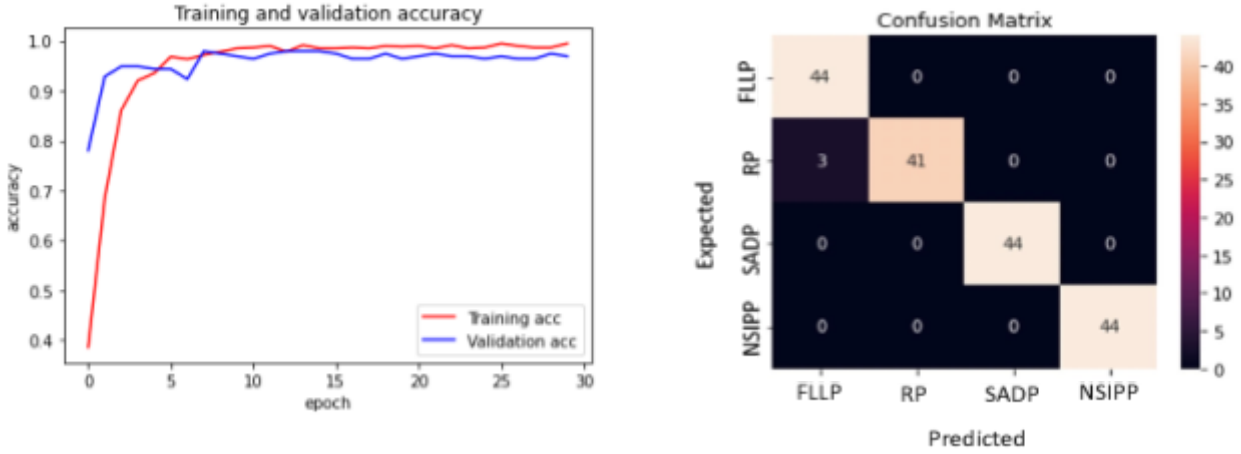

(a) (b)

Single-Stage Model

The accuracy results for the MobileNetV2 architecture are shown in Fig. 6a. The training phase had an accuracy of 99.80%, and the validation phase had an accuracy of 99.0%. As shown in Fig. 6b, the confusion matrix for the test phase indicates an accuracy of 99.20%. The model correctly classified 60 slices as NSIPP and 60 slices as SADP, but it made two errors by confusing FLLP and RP.

Figure 4 - Accuracy of MobileNetV2 in the training and validation sets with the classification model for the expiration exam (99.0% validation accuracy in the 6th epoch) (b); Confusion matrix of MobileNetV2 test step for expiration classification with 90.8% accuracy. NonSADP = non-small airway disease pattern; SADP = small airway disease pattern (b)

(a) (b)

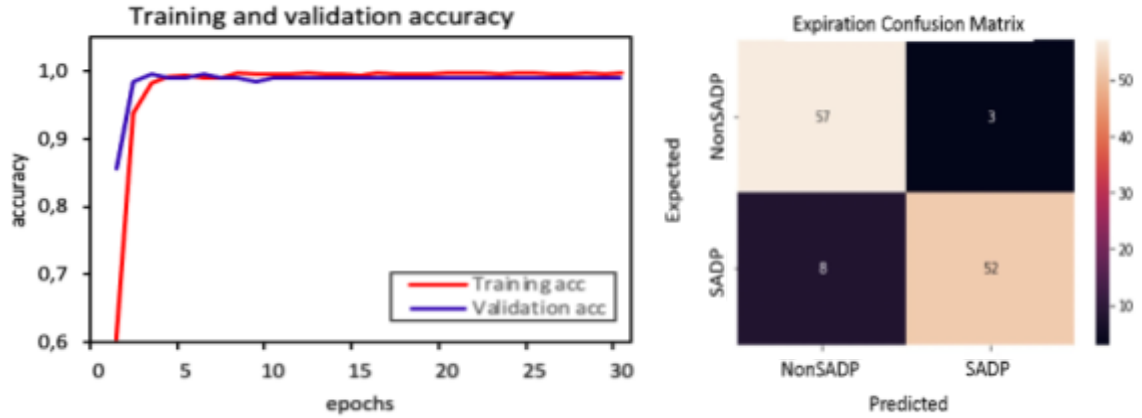

Figure 5 - Accuracy of MobileNetV2 in the training and validation sets with the classification model for the inspiration exam (98.0% validation accuracy in the 12th epoch) (a); Confusion matrix of the MobileNetV2 test step for inspiration classification with 99.6% accuracy. FLLP = fibrosis-like lesion pattern; NSIPP = nonspecific interstitial pneumonia pattern; RP = resorption pattern; SADP = small airway disease pattern (b)

(a) (b)

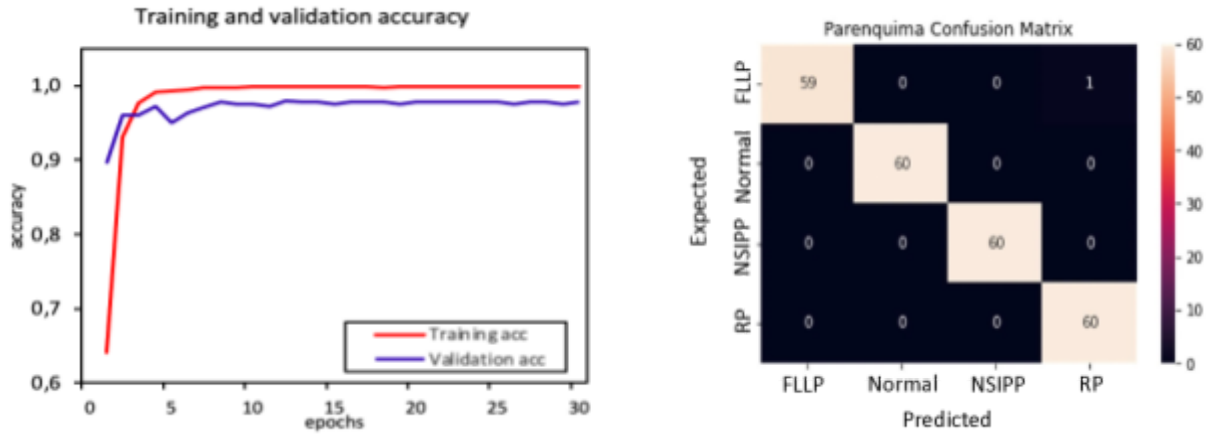

Application of the Single-Stage Model in a Sample of Eight Patients

In the next research step, we used the single-stage model to analyse complete CT exams of patients with post-COVID-19 patterns. Instead of analysing slices from different patients, the model looked at sequential slices from a single patient. We randomly selected eight patients from a database of 87, anonymized their exams, and assigned them numbers one through eight. These patients exhibited the following patterns: RP (Patients 3, 5, 6 and 8), SADP (Patients 3 and 7), and FLLP (Patients 1,2,4 and 6). The model's accuracy was 100% for Patient 1 with FLLP (Fig 7a), Patient 3 with RP/SADP (Fig 7b), Patient 6 with FLLP/RP (Fig 7c) and Patient 7 with SADP (Fig 8a). For Patient 4 with FLLP (Fig 8b), the accuracy was 93.46%, but some slices were confused with RP. The accuracy for Patients 5 and 8 with RP was 80% (Fig 8c and 9a).

Figure 6 - Accuracy of MobileNetV2 in the training and validation sets with the direct classification model for post-COVID patterns (99.0% in the 8th epoch) (a) and Confusion matrix of the MobileNetV2 test step in direct modelling (99.20% accuracy). FLLP = fibrosis-like lesion pattern; NSIPP = nonspecific interstitial pneumonia pattern; RP = resorption pattern; SADP = small airway disease pattern(b)

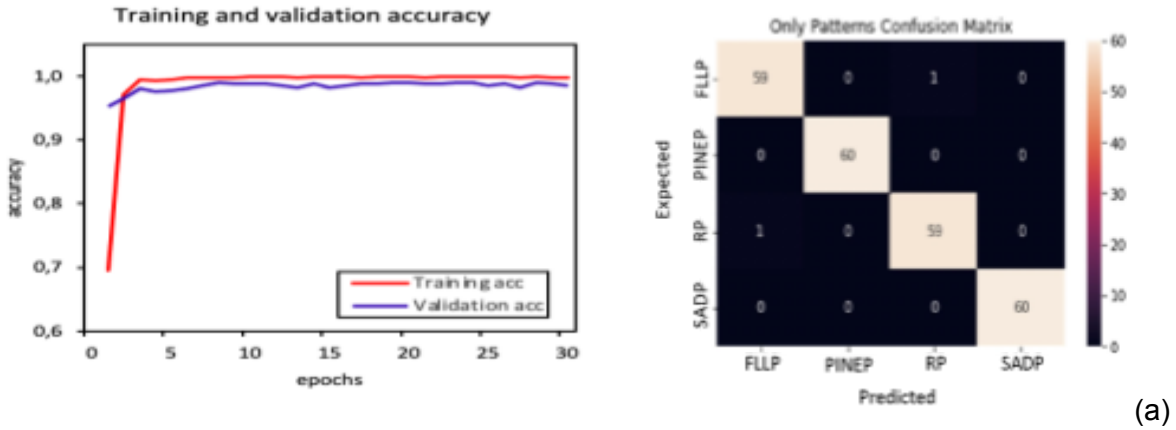

(a)

(b)

Figure 7 - Confusion matrix for Patient 1 in the direct classification model of post-COVID patterns – 100% accuracy. FLLP = fibrosis-like lesion pattern; RP = resorption pattern; SADP = small airway disease pattern (a); Confusion matrix for Patient 3 in the direct classification model of post-COVID patterns – 100% accuracy. FLLP = fibrosis-like lesion pattern; RP = resorption pattern; SADP = small airway disease pattern (b); Confusion matrix of Patient 6 in the direct classification model of post-COVID patterns – 100% accuracy. FLLP = fibrosis-like lesion pattern; RP = resorption pattern; SADP = small airway disease pattern (c)

(a) (b) (c)

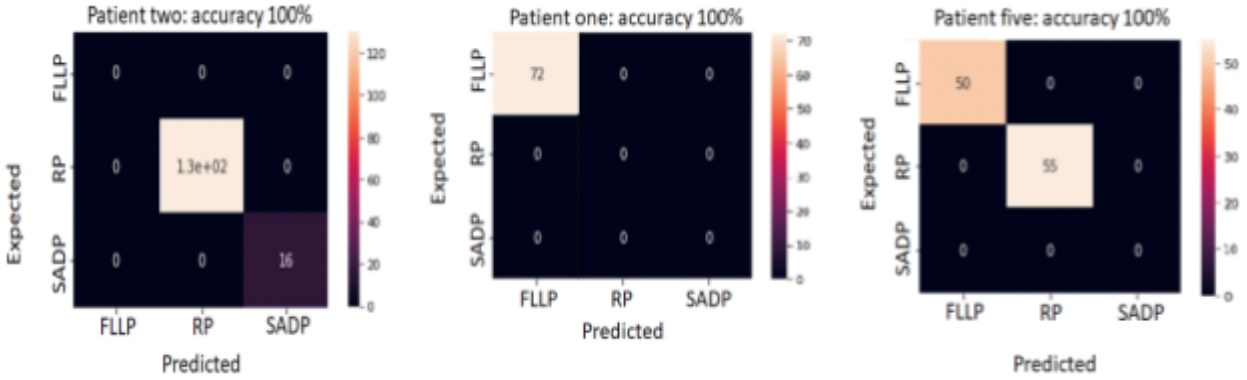

Figure 8 - Confusion matrix for Patient 7 (a); Patient 4 (b) and Patient 5 (c) in the direct classification model of post-COVID patterns – 100% accuracy. FLLP = fibrosis-like lesion pattern; RP = resorption pattern; SADP = small airway disease pattern (a); Confusion matrix for Patient 4 in the direct classification model of post-COVID patterns – 93.46% accuracy. FLLP = fibrosis-like lesion pattern; NSIPP = nonspecific interstitial pneumonia pattern; RP = resorption pattern; SADP = small airway disease pattern (b); Confusion matrix for Patient 5 in the direct classification model of post-COVID patterns – 80% accuracy. FLLP = fibrosis-like lesion pattern; RP = resorption pattern; SADP = small airway disease pattern (c).

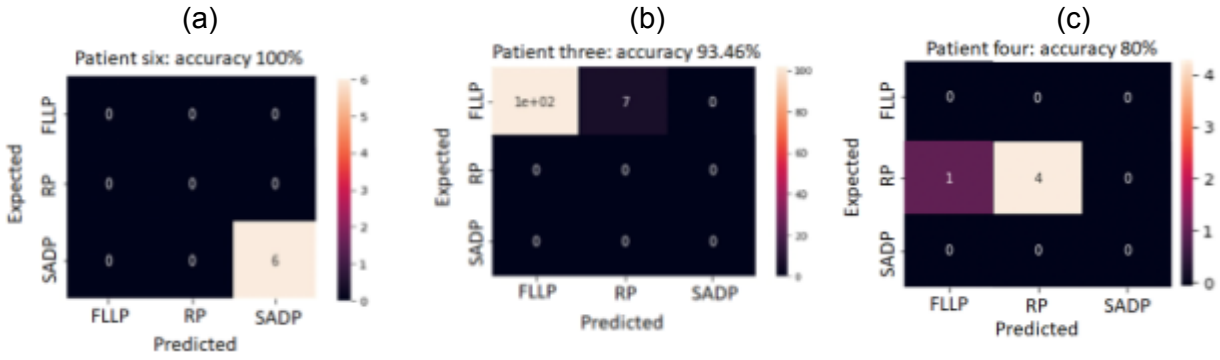

Patient 2 had patterns of resorption (PR) and fibrosis-like lesions (FLLP) (Fig 9b), with an accuracy of 75,63%. Overall, the single-stage model had an average accuracy of 91.14% in detecting the three post-COVID-19 patterns RP, FLLP, and SADP.

Figure 9 - Confusion matrix of Patient 8 in the direct classification model of post-COVID patterns – 80% accuracy. FLLP = fibrosis-like lesion pattern; RP = resorption pattern; SADP = small airway disease pattern (a); Confusion matrix for Patient 2 in the direct classification model of post-COVID patterns – 75.63% accuracy. FLLP = fibrosis-like lesion pattern; RP = resorption pattern; SADP = small airway disease pattern(b)

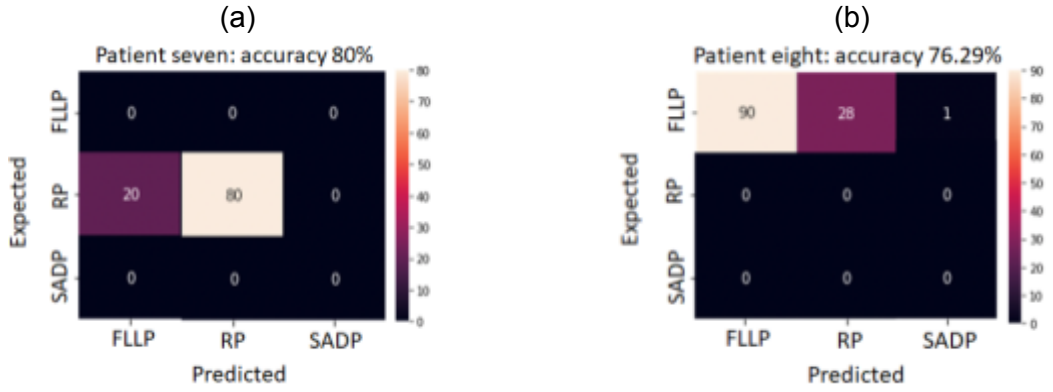

Discussion

The goal of the models was to use AI to recognize fixed patterns. These AI algorithms work best when there are few diagnostic options and consistent criteria reproducible by radiology. Developing the models was challenging because we had

to balance the available images for each abnormal and normal pattern and enable learning with a small number of images in each class (post-COVID pattern). However, we achieved this through augmentation techniques and transfer learning. Although this is only a preliminary work, adding more images to the model's development database can improve its performance. The accuracy of the model for identifying the patterns in the slices was excellent, giving us great hope for the models' performance with complete exams. In the second part of the study, a sample of eight chest CT scans was used to simulate the process of reading exams from a worklist. However, to fully identify the strengths and weaknesses of the models, a more significant number of exams must be analysed using this methodology. It involves studying each case analysed by the models to determine situations where AI is ineffective. Despite the limited number of exams in the second part, the results were excellent and broadly consistent with the results of tests using only slices. One limitation of the complete exam tests was the lack of NSIPP.

It is important to note that the pandemic is currently less severe than it was in 2020. This means that cases are less severe, with fewer symptoms and complications compared to that time. To ensure accurate modelling, it is necessary to update the database to reflect the changes in radiological profiles resulting from successful immunization efforts.

After examining the results and images of the second test's eight cases, we found that the model sometimes had difficulty distinguishing between resorption patterns and lesions resembling fibrosis in specific slices. This issue arose when analysing the slices of Patients 3, 7, and 8, particularly in areas without significant architectural distortion where the densities of the lesions are similar. In addition, ground-glass opacities, present in classical fibrosing interstitial diseases, can indicate an early phase of fibrosis. The model mimics the challenges that radiologists face daily, including the difficulty distinguishing between similar lesions. Even experienced radiologists can make mistakes in these cases, and different radiologists may have varying opinions. In the group of eight patients, it was noticed that the RP and PLSF patterns did not occur together. This finding is essential for identifying the model's accuracy in cases where these patterns must be distinguished.

It is important to note that when CT scans show less severe patterns, such as in Patients 5 and 8, it can be more challenging for the model to diagnose accurately. Typically, models are developed using slices with clear patterns, but this is not always the case in real life. Despite this, the model still had a high success rate of 80% for these patients' scans.

One limitation of the model when analysing a complete exam is that it assigns diagnoses slice by slice and does not produce a single diagnosis. By identifying all patterns in all slices, there is no room for doubt about the diagnosis of the model. However, although the accuracy was high, as occurred in Patients 2, 4, 5, and 7, it was not 100%. There were some misdiagnoses in specific slices that contained the smallest parts of the lesion. However, in cases with a second pattern present, it may only appear in a few slices and not be deemed an error. Therefore, it is ideal for future models to assign importance to the findings of each slice. When analysing patterns, humans use a Cartesian approach but integrate all impressions to form a unique impression of an exam. The next step in improving these models is to make the analysis more similar to how a radiologist thinks.

Conclusions

Three different AI models have been successfully developed to read post-COVID-19 patterns on CT scans, and their results have been considered excellent from a diagnostic interpretation point of view. The CT findings were consistent with those described in the literature. They represent a period in the pandemic between July 2021 and May 2022, when immunization effects were already present and affected the presentation of COVID-19. Although the complete exam tests showed excellent results with a small sample, improvements are needed to integrate all the information obtained into a single diagnosis.

Acknowledgements

This work was carried out with the support of the The National Council for Scientific and Technological Development - CNPq 308717/2020-1, the Coordination for the Improvement of Higher Education Personnel - Brazil (CAPES) - Funding Code 001 and CAPES 88881.506840/2020-01.

References

1. Cau R, Faa G, Nardi V, Balestrieri A, Puig J, Suri JS, SanFilippo R, Saba L. Long-COVID diagnosis: from diagnostic to advanced AI-driven models. Eur J Radiol. 2022. 148:110164.

2. Luqmani Y.A., El Hashim A. The COVID-19 pandemic: a health crisis managed or a panic response with disastrous future consequences? Med Princ Pract.2022. 31:1-10.

3. British Thoracic Society (2020) British thoracic society guidance on respiratory follow up of patients with a clinico-radiological diagnosis of COVID-19 pneumonia. 2020.

4. Nalbandian A, Sehgal K, Gupta A et al. Post-acute COVID-19 syndrome. Nat Med. 2021. 27:601-615.

5. Caruso D, Guido G, Zerunian M et al. Post-acute sequelae of COVID-19 pneumonia: six-month chest CT follow-up. Radiology. 2021. 301:E396-E405.

6. Desai AD, Lavelle M, Boursiquot BC, Wan EY. Long-term complications of COVID-19. 2022, 322:C1-C11.

7. Lee KS, Wi YM. Residual lung lesions at 1-year CT after COVID-19. 2022. Radiology 302:720-721.

8. Alhasan M, Hasaneen M. Digital imaging, technologies and artificial intelligence applications during COVID-19 pandemic. Comput Med Imaging Graph. 2021. 91:101933.

9. Noce J, Chantong G, Jauregui G, Mogami R, Monteiro A, Figueiredo K, Vellasco M. Applied enhanced Q-NAS for COVID-19 detection in CT images. In: Mahmud CIM, Kaiser MS, Mammone N, Morabito FC (eds) Applied intelligence and informatics. Springer, Berlin, Germany 2023. p 419.

10. Leão PPS, Freire NS, Pinto RA, Maciel K, Pinto B, Giusti R, Santos EM, Detecção de Covid-19 em Imagens de Raio-x Utilizando Redes Convolucionais, J. Health Inform. 2020 Número Especial SBIS - Dezembro: 393-8

11. Simonyan, K. and Zisserman, A. Very deep convolutional networks for large-scale image recognition, NASA/ADS. 2014.

12. Sandler M, Howard A, Zhu M, Zhmoginov A, Chen LC. MobileNetV2: Inverted Residuals and Linear Bottlenecks, 2018 IEEE/CVF Conference on Computer Vision and Pattern Recognition, Salt Lake City, UT, USA. 2018. pp. 4510-4520.

13. Friedman B, Nissenbaum H. Bias in computer systems. ACM Trans Inf Syst. 1996. 14:330-347.

14. Mehrabi N, Morstatter F, Saxena N, Lerman K, Galstyan A. A survey on bias and fairness in machine learning. ACM Comput Surv.2021. 54:1-35.

15. Chlap P, Min H, Vandenberg N, Dowling J, Holloway L, Haworth A. A review of medical image data augmentation techniques for deep learning applications. J Med Imaging Radiat Oncol. 2021. 65:545-563.

16. Goodfellow I, Yoshua B, Courville A. Deep learning. The Mit Press. 2016., Cambridge, US

17. Mogami R, Lopes AJ, Filho RCA, De Almeida FCS, Messeder A, Koifman ACB, Guimarães AB, Monteiro A. Chest computed tomography in COVID-19 pneumonia: a retrospective study of 155 patients at a university hospital in Rio de Janeiro, Brazil. Radiol Bras.2021. 54:1-8.

18. Mogami R, Filho R.C.A., Chantong C.G.C. et al. The importance of radiological patterns and small airway disease in long-term follow-up of postacute COVID-19: a preliminary study. Radiol Res Pract.2022. 2022:7919033.